The preadsorbed water-promoted mechanism of the Water-Gas Shift reaction

Constantinos D. Zeinalipour-Yazdi and Angelos M. Efstathiou**

Heterogeneous Catalysis Laboratory, Department of Chemistry, University of Cyprus, CY 1678, Nicosia, Cyprus

* Corresponding Authors. E-mail address: zeinalip@ucy.ac.cy, (C.D. Zeinalipour); efstath@ucy.ac.cy (A.M. Efstathiou)

TITLE RUNNING HEAD: The preadsorbed water-promoted mechanism of the WGS reaction

Abstract

In this work, a detailed first principle study of the mechanism of the heterogeneous catalytic Water-Gas Shift (WGS) reaction on a rhodium cluster is presented. A large number of possible reaction mechanisms relevant to the WGS reaction are explored, and as many as 34 possible pathways are located due to the unsaturated nature of the metal cluster and the multitude of intermediate species binding configurations. Brønsted-Evans-Polanyi relationships and the Sabatier principle are used to locate the *kinetic* and *thermodynamic* paths occurring on the rhodium cluster. A detailed potential energy diagram of the kinetically favoured mechanism is presented that shows that the RDS of the reaction are the water dissociation, formate association and formate decomposition elementary reactions, with free energy barriers ($\Delta G^{\ddagger}$) of 24.2, 25.9 and 27.0 kcal/mol, respectively. The poisoning effect of co-adsorbed CO and the beneficial effect of preadsorbed water on the kinetic rate of this reaction is demonstrated and a water-mediated mechanism is proposed. In the water-mediated mechanism

favourable H-bonding interactions stabilize Zundel-cations adsorbed to the metal cluster, which manifest a lower energy path for the dissociation of water. Participation of co-adsorbed water in this mechanism explains the promoting effect water vapour pressure has on the reaction kinetics (positive reaction order with respect to water) by lowering the free energy of the rate-determining step barrier by 4.0 kcal/mol and causing a 10-fold increase of the reaction rate for the water dissociation elementary reaction step. In addition a presumable preadsorbed water-mediated mechanism is shown to have an even lower free energy barrier (16.9 kcal/mol) causing a 2000-fold increase of the elementary reaction rate for water dissociation. It is suggested that operation of heterogeneous WGS catalysts in a cyclic fashion where water is first preadsorbed might enhance current catalyst performance and CO conversion turnover frequencies.

Keywords: Water-gas shift reaction; Rh catalyst; DFT; catalytic reaction mechanisms.

1. Introduction

In recent years, there has been a renewed interest in the heterogeneous catalytic water-gas shift (WGS) reaction, $CO + H_2O \leftrightarrow CO_2 + H_2$, due to the need for pure hydrogen production compatible with hydrogen-operated fuel cell power generation systems.[1] Such technologies have gained increasing respect in the light of developments of hydrocarbon steam-reforming technologies for which natural gas and other biomass-derived liquid fuels, such as ethanol, sugars and bio-oil can efficiently be used to produce syngas and hydrogen. [2-5] The reduction in the CO content of syngas (CO/H_2 mixture) is industrially achieved in a two-step process that involves a high- and a low- temperature step. The high-temperature shift (~310-450°C) reduces the CO concentration from 10 to 3 vol% with the use of Fe_3O_4/Cr_2O_3 catalysts. The low-temperature shift (~180-250°C) reduces the CO content to 500 ppm with the use of $Cu/ZnO/Al_2O_3$ catalysts.[6-8] The low-

temperature catalyst is pyrophoric and deactivates if exposed to air[7]; thus, attempts now have focused in finding catalysts that are non-pyrophoric with high activity at low-temperatures, and able to minimize the CO content of hydrogen to concentrations less than 5 ppm.[1]

For a heterogeneous catalytic reaction, first-principle computations can be readily employed for catalysts screening. [9-11] A key component in this procedure is the precise knowledge of the kinetically favored reaction path for the particular reaction of interest. One of the important aspects in the elucidation of the WGS reaction mechanism is the identification of the structure of the *formate* imtermediate, which could be of a bidentate (**bi-COOH**), unidentate (**uni-COOH**) or carboxylate (**carb-COOH**) chemical structure according to Fig.1. [12, 13]

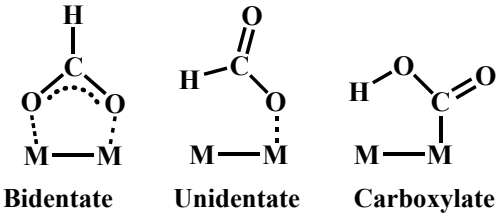

Figure 1: Chemical structures of formate species found on transition metals.

Recently, a detailed mechanism of the WGS reaction has been proposed by Mavrikakis and co-workers for the (111) surface of Cu[14] and Pt[13], where the authors suggest the participation of an active carboxylate-formate intermediate in the reaction path. A similar key intermediate was previously found by Goddard and co-workers for the direct methanol oxidation mechanism.[15] There is a limited number of other first principles studies that explore the WGS reaction mechanism on other transition metal surfaces or clusters. In particular, Liu *et al.*[16] examined the mechanism on Au/CeO_2 model catalyst and suggest that the reaction pathway occurs on a four to six atom Au

cluster. Furthermore, first principle studies of the WGS reaction on molybdenum carbide surfaces showed that the rate-determining step (RDS) is the oxidation of CO to carbon dioxide[17], and that a surface oxycarbide promotes the reaction rate.[18] Liu *et al.*[19] investigated the WGS reaction on Cu_{29} and Au_{29} nanoparticles and Cu(111) and Au(111) surfaces. They have suggested that the WGS reaction on these systems operates either via a redox or associative carboxylate-formate mechanism and that the RDS is that of the dissociation of water.

In the present work, we propose a new water-mediated mechanism that explains various previous findings with respect to the kinetics of the WGS reaction on rhodium nanoclusters. We use a highly uncoordinated tetratomic rhodium cluster to show that the reaction mechanism and the turnover frequency of the catalytic cycle may proceed on the metal cluster through an associative carboxylate-formate mechanism, similar to that recently reported on Cu(111) and Pt(111) single crystal surfaces.[12, 13] The RDS in this reaction mechanism are the water dissociation, formate association and formate dissociation elementary reactions that have pronounced activation barriers. It is shown that the rate of water dissociation is enhanced through a water-mediated mechanism in which co-adsorbed water promotes the water dissociation elementary reaction step. In particular, it was found that co-adsorbed water can lower the activation energy barrier for the dissociation of an adjacent water molecule as a result of the hydrogen bonding interactions that weaken the O-H bond. Furthermore, the poisoning effect of preadsorbed CO on the catalytic activity of the heterogeneous WGS reaction due to stronger adsorption and electronic effects is discussed.

2. Computational Methodology

Restricted and unrestricted Density Functional Theory (DFT) computations are employed, as implemented in Gaussian 03,[20] with the use of Becke's three-parameter

hybrid exchange functional[21] (XC) combined with the Lee-Yang-Parr non-local correlation functional[22], abbreviated as B3LYP. This XC functional predicts the correct adsorption site for CO in cases where LDA and GGA have previously shown to fail.[23, 24] We adopted a computational strategy whereby all structures were first fully optimized at UB3LYP/CEP-121G(Rh),aug-cc-pVTZ(C,O,H) level of theory, to find all possible configurations (e.g. linear, bridged, hollow) of the various adsorbed intermediates (e.g. H, CO, OH, H_2O, COOH) of the WGS reaction. Full optimization was critical since strong adsorption induced structural changes to the transition metal cluster $Rh_4(3,1)$ were observed. Basis set saturation was tested for CO adsorption onto $Rh_4(3,1)$ (see Table 1) using Dunnings' correlation consistent augmented valence triple zeta basis sets[25-29], which show that basis sets larger than aug-cc-pVTZ result only in small oscillations of the adsorption energy. The good agreement between the basis set superposition error (BSSE) corrected adsorption energies and the non-BSSE corrected values suggest that corrections by the counterpoise method of Boys and Bernardi[30] are not necessary for this particular basis set model system. Furthermore, this basis set is generally known to be appropriate when intermolecular interactions, such as H-bonding and dipole-dipole interactions, are important between adsorbed intermediates. Linear dependencies of the basis functions were removed by using the spherical version (5d and 7f) of this basis set. For the $Rh_4(3,1)$ cluster the Stevens/Basch/Krauss Effective Core Potential (ECP) triple-split basis was used, denoted as CEP-121G.[31-33] The CEP-4G and CEP-31G were also examined but no differences in the total energies were observed. The SCF convergence criteria for the root mean square (rms) density matrix and the total energy were set to 10^{-8} Hartree/bohr and 10^{-6} Hartrees, respectively. For all computations that had open and

closed shell electronic configurations the spin multiplicity was set to two and one, respectively. Open shell computations were examined for spin contamination, which was found to be negligible.

Table 1: Basis set saturation test for CO adsorption on $Rh_4(3,1)$

H_2O basis set	**$\Delta E_{non\text{-}BSSE}$** (kcal/mol)	**ΔE_{BSSE}** (kcal/mol)	**ΔH^b** (kcal/mol)
aug-cc-pVDZ	-38.4	-38.5	-37.1
cc-pVTZ	-38.5	-38.9	-37.2
aug-cc-pVTZ	-39.6	-39.3	-38.3
cc-pVQZ	-39.1	-39.3	-37.3
aug-cc-pVQZ	-40.4	-39.5	-39.1
Exp.[a]			**-39.43**

[a] Smedh *et al.*[34] (TDS of CO on Rh/Al_2O_3)
[b] computed at standard temperature and pressure (298K, 1atm)

The potential energy surface (PES) diagrams of the various mechanistic paths were obtained by full relaxation of the various possible cluster-intermediate complexes using the relationship:

$$\Delta E = E_{M-X} - E_{M-(COg,H_2Og)} \qquad (1)$$

where, ΔE is the total energy change for the reactants in their reference state ($CO_{(g)}$, $H_2O_{(g)}$) in order to form the various adsorbed intermediates, E_{M-X} is the energy of the nanoparticle with adsorbed intermediates, and $E_{M-(COg,H_2Og)}$ is the energy of the cluster and gas phase reactants restricted at a separation by a distance of 10Å. Similar relationships were used for the enthalpy change (ΔH) and the Gibbs free energy change (ΔG). Local minima for the reaction intermediates and transition states (TS) have been confirmed by vibrational analysis, by the absence and presence of one vibrational frequency, respectively. Transition state structures were either located using the

Synchronous Transit-Guided Quasi-Newton (STQN) method of Schlegel and co-workers[35, 36] or by scanning a particular bond length at a 0.05 Å resolution and relaxing the remaining atoms. The imaginary frequency of the located TS was animated using MOLEKEL[37] to ensure that it corresponds to the desired reaction coordinate. Infrared spectra simulations were performed within the harmonic oscillator approximation. The infrared intensity of each vibrational mode *i* was taken to be proportional to the square of the derivative of the molecular dipole field with respect to the vibrational coordinate, q_i:

$$\left[\int \psi_{v=0} \frac{\partial \boldsymbol{\mu}}{\partial q_i} \psi_{v=1} dq_i \right]^2 \qquad (2)$$

where the harmonic oscillator wavefunctions are used for $\psi_{v=0}$ and $\psi_{v=1}$. The dipole derivatives are calculated analytically, together with the force constants from the DFT wavefunction.[38]

3. Results and Discussion

3.1 WGS reaction adsorbed intermediate species

Initially an extensive search of the chemically possible reaction intermediates (e.g. CO, H, COOH, H_2O and OH) of the WGS reaction on $Rh_4(3,1)$ was performed. In this search various initial structures and adsorption configurations (e.g. linear, bridged and hollow) were considered, and ten stable intermediate species were located (see Fig. 2). For these intermediates the total energy (ΔE), enthalpy (ΔH) and Gibbs free energy (ΔG) change has been computed and the trends obtained are presented in Fig. 3. The pronounced adsorption energy differences observed among the various adsorption configurations of the same intermediate suggest that consideration of the local binding

configuration (e.g. linear, bridged, hollow) of a particular reaction intermediate in the modeling of the reaction path is necessary. Furthermore, the similar trend observed in ΔE, ΔH and ΔG of these intermediates indicates that vibrational and rotational energy effects among the various adsorbed intermediates are similar, and thus these can be omitted in the search of the kinetically fastest reaction path, but they will be subsequently considered during the explicit computation of the free energy barrier of the kinetically fastest reaction path.

In the following sub-section we provide a detailed description of the adsorption energetics and spectroscopic identification of the fourteen stable intermediates (see Fig. 2) computationally located on $Rh_4(3,1)$ cluster.

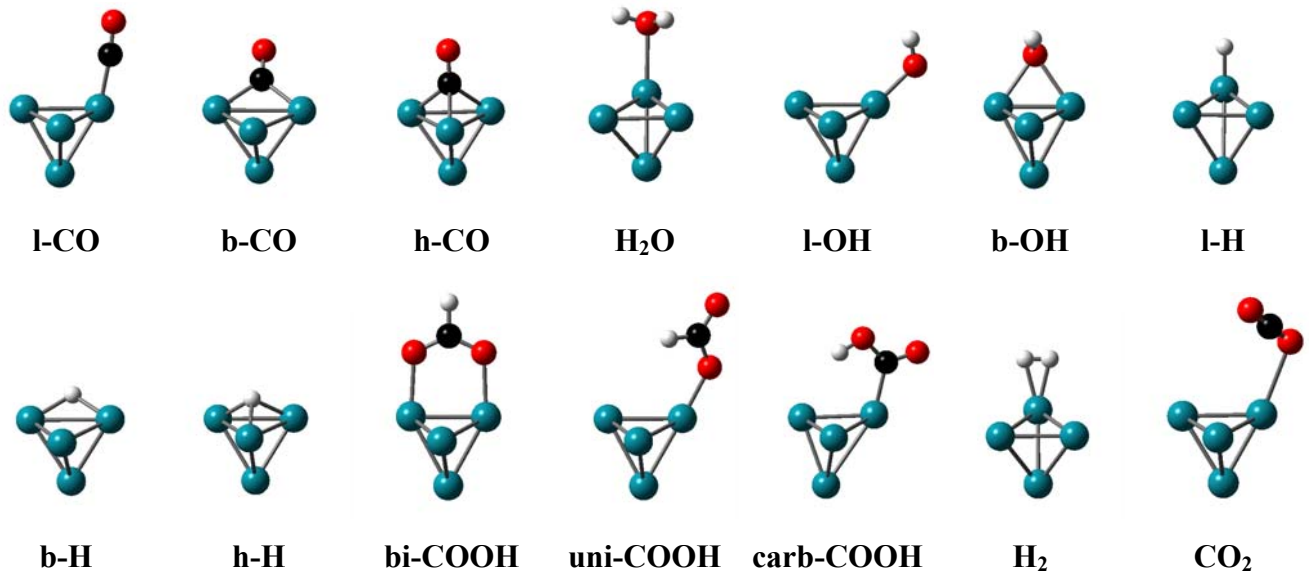

Figure 2: Molecular geometries and labels of stable intermediates found for the WGS reaction on $Rh_4(3,1)$. All -H, -OH and -COOH intermediates have open shell electronic configurations (spin = ½). Black, dark grey, grey and white correspond to carbon, oxygen, rhodium and hydrogen, respectively. The cartesian coordinates of the relaxed cluster-intermediate molecular geometries are given in the supporting information (S-Table 1a).

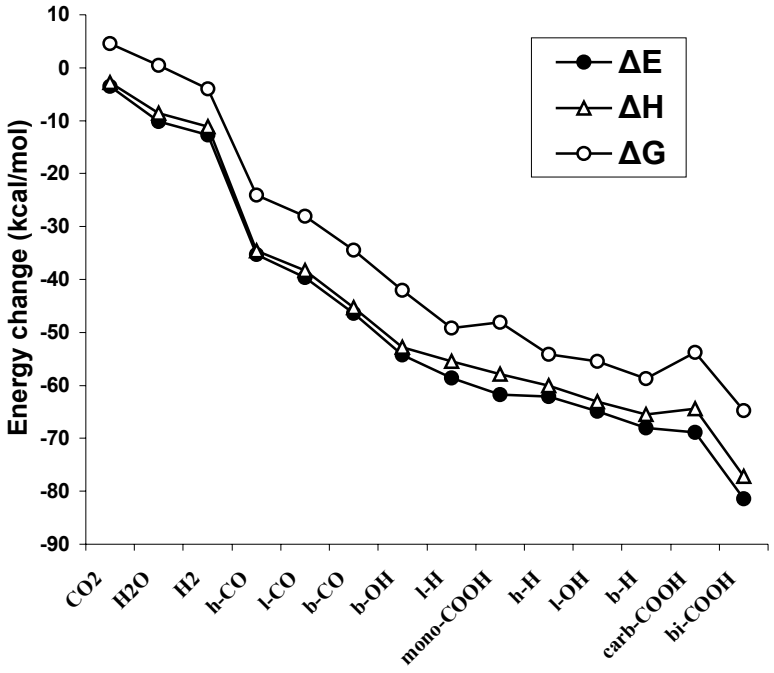

Figure 3: Adsorption energies (ΔE), enthalpies (ΔH) and Gibbs free energy (ΔG) changes for the various intermediate species of the WGS reaction on $Rh_4(3,1)$ cluster at standard temperature and pressure (STP). All energies presented in this graph are given in the supporting information (S-Table 2).

3.1.1 Adsorbed CO (CO_{ads})

Five distinct binding configurations (linear, bridged, hollow, dicarbonyl, tricarbonyl) of carbon monoxide (CO) on $Rh_4(3,1)$ were found. These are expected to exist on any transition metal cluster that exhibits low coordination. As previously shown[39, 40], these binding configurations can be identified spectroscopically by diffuse reflectance infrared Fourier-transform spectroscopy (DRIFTS) on supported rhodium catalysts. Linear CO (**l-CO**) has an adsorption free energy of -39.3 kcal/mol in agreement with the value of -39.43 kcal/mol determined from temperature-programmed-desorption (TPD) spectroscopy of CO on Rh/Al_2O_3.[34] **l-CO** binds almost perpendicularly to the surface of the Rh cluster, through its carbon end. Bridged (**b-CO**) and hollow CO (**h-CO**) have adsorption energies of -62.5 and -52.2 kcal/mol, respectively. Dicarbonyl (**di-CO**)

and tricarbonyl (**tri-CO**) intermediate species exhibit adsorption energies close to that of linear CO, and therefore are not considered since similar reaction energetics compared to **l-CO** are expected. Consequently, the CO adsorbed intermediates considered for modeling the WGS reaction path were **l-CO**, **b-CO** and **h-CO**. The adsorption energetics of CO with respect to the water-preadsorbed Rh clusters showed differences in adsorption energy of CO to be less than a few tenths of a kcal/mol, suggestive of an absence of water-preadsorbed enhancement of CO adsorption.

3.1.2 Adsorbed water (H_2O_{ads})

Our computations indicate that water can adsorb both molecularly and dissociatively on the $Rh_4(3,1)$ cluster. Temperature-programmed electron-energy-loss (TP-EEL) of water onto Rh(100) at low temperatures showed molecular adsorption as suggested by the characteristic HOH scissor motion (1653cm^{-1}) and OH stretching (3065-3307cm^{-1}) vibrational modes.[41] Molecular adsorption of water follows a barrier-less energetic path that results in a flat-top configuration of H_2O with respect to the (111) cluster face, in agreement with previous computational studies.[42-44] We find a Rh-O bond length of 2.34 Å and a tilt angle of about 80˚ with respect to vertical (see Fig. 2). The computed adsorption energy for water (-10.1 kcal/mol) is in agreement with the values obtained from secondary ion mass-spectrometry (SIMS) studies of water adsorption on polycrystalline rhodium[45], and temperature-programmed desorption (TPD) on Rh(100)[46] that yielded adsorption energies of -11.0 and 11.3 kcal/mol, respectively. It is known from low-energy-electron-diffraction (LEED) experiments on Rh(111) that water forms a ($\sqrt{3}$x$\sqrt{3}$)R30˚ bilayer[47] with a nearest-neighbor distance of 4.66 Å. This H-bonded bilayer[48] causes additional stabilization of water onto the transition metal surface, evident

by the 10% increase of experimental[45, 46] compared to the present computed adsorption energies.

3.1.3 Adsorbed hydroxyl (OH_{ads}) *and atomic hydrogen* (H_{ads})

Adsorbed water dissociates into hydroxyl (OH_{ads}) and atomic hydrogen (H_{ads}) intermediate species. In particular, for OH_{ads} we find a linear (**l-OH**) and bridged (**b-OH**) binding configuration to be stable on the $Rh_4(3,1)$ cluster with adsorption energies of -64.8 and -54.3 kcal/mol, respectively. For the Rh-O bond of **l-OH** and **b-OH**, bond lengths of 1.91 and 2.13 Å were found, respectively (see Fig. 2). Subsequent dissociation of hydroxyl into atomic oxygen (O_{ads}) and hydrogen (H_{abs}) species is not considered as a possible low-T WGS elementary reaction step, since such a dissociation is highly unlikely at $T < 400$ K.[45] For this reason, a plausible redox WGS mechanism where CO is directly oxidized by atomic oxygen is not considered is this study. For the H_{ads} species we find linear (**l-H**), bridged (**b-H**) and hollow (**h-H**) atomic hydrogen as stable binding configurations, with adsorption energies of -58.6, -68.1 and -62.1 kcal/mol, respectively. The Rh-H bond length is found to be 1.54, 1.70 and 1.78 Å for **l-H**, **b-H** and **h-H**, respectively.

3.1.4 Adsorbed Formate ($COOH_{ads}$)

Formates are stable intermediates ($COOH_{ads}$) on the $Rh_4(3,1)$ cluster at STP, stabilized either in a classical bidentate (**bi-COOH**) or the less commonly identified unidentate (**uni-COOH**) and carboxylate (**carb-COOH**) chemical structure. Bidentate formate (**bi-COOH**) species are known to form on rhodium from time-resolved electron energy-loss (TREEL) studies[41] identified by the OCO scissor ($\delta_{(OCO)} = 758$ cm^{-1}) and symmetric stretching ($\nu_{s(COO)} = 1323$ cm^{-1}) vibrational modes in good agreement with the

computed values of $\delta_{(OCO)}$ = 771 cm^{-1} and $\nu_{s(COO)}$ = 1348 cm^{-1}. Spectroscopic techniques (transmission IR, DRIFTS) have claimed that a formate intermediate (COOH) is present during the WGS reaction on metal oxides (MgO [49], ZnO [50] and CeO_2 [51]) and on metal supported catalysts (Rh/CeO_2 [52], Pt/MgO [53], Pt/CeO_2 [54]). However, in most of the experimental studies it is still unclear which type of formate is a true active intermediate (as opposed to just a spectator species) and whether the active intermediate is located at the metal, the substrate or even at their interface. [55]

In Fig.4, the simulated IR absorption spectra for the various possible $COOH_{ads}$ species are presented. It is evident that bidentate formate can be spectroscopically identified by the absence of an intense band around ~1735cm^{-1}, which is present in **uni-COOH** and **carb-COOH**. On the other hand, considering that the full width at half maximum (FWHM) of absorption bands in IR spectroscopy of surfaces normally ranges between 50-100 cm^{-1}, the only band that can be differentiated between **uni-COOH** and **carb-COOH** is the CH stretch ($\nu_{(C-H)}$ = 2898cm^{-1}) and the hydroxyl stretch ($\nu_{(O-H)}$ = 3701cm^{-1}) with the latter being relatively weak and in most experiments the $\nu_{(O-H)}$ overlaps with the stronger hydroxyl stretching bands of water. Therefore, the spectroscopic identification of the two intermediates (**uni-COOH**, **carb-COOH**) is difficult to be established by experiment.

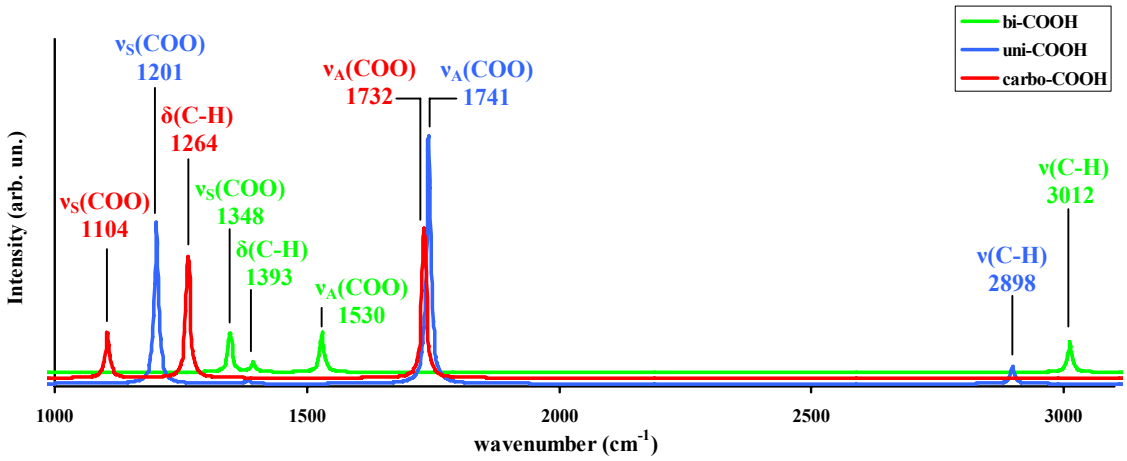

Figure 4: Simulated Infrared spectra of the carboxylate, bidentate and unidentate formate.

3.1.6 Adsorbed molecular hydrogen (H_{2ads}) and carbon dioxide (CO_{2ads})

Our computations revealed that molecular hydrogen adsorbs in a parallel-atop configuration with respect to the $Rh_4(3,1)$ cluster at a distance of 1.75 Å. The adsorption energy at STP was found to be relatively high, -12.7 kcal/mol, thus we expect this intermediate to take part during the associative desorption of molecular hydrogen from the surface. Molecular carbon dioxide also weakly binds in a tilt-atop configuration to the Rh cluster through one of the filled orbitals at the oxygen with an adsorption energy of -3.6 kcal/mol and a Rh-O bond of 2.50 Å. Adsorption of molecular H_2 and CO_2 is known from LEED experiments on Rh(111), where adlayers of (1x1) and (√3x√3)R30° symmetry have been observed, respectively.[56]

3.2 Mechanism of the low-T WGS reaction

Based on the various reaction intermediates computationally explored and confirmed from experimental studies, one can postulate the following elementary

reaction steps for the WGS reaction on a rhodium transition metal cluster at *low temperatures*[57]:

CO adsorption: $CO_{(g)} + H_2O_{(g)} + * \rightarrow CO* + H_2O_{(g)}$

H_2O adsorption: $CO* + H_2O(g) + * \rightarrow CO* + H_2O*$

H_2O dissoc.: $CO* + H_2O* + * \rightarrow CO* + H* + OH*$

Formate assoc.: $CO*+H*+OH* \rightarrow COOH*+H*+ *$

Formate dissoc.: $COOH* + H* \rightarrow CO_2* + 2H*$

H_2 *association:* $CO_2* + H* + H* \rightarrow CO_2* + H_2*+ *$

H_2 *desorption:* $CO_2* + H_2* \rightarrow CO_2* + H_{2(g)} + *$

CO_2 *desorption:* $CO_2* + H_{2(g)} \rightarrow CO_{2(g)} + H_{2(g)} + *$

The fact that there is a multitude of binding modes of a particular adsorbed intermediate suggests that there is a large number of possible reaction pathways one has to examine for the WGS reaction on small-dimensional clusters. For simplicity, on a relatively defect free surface one could only consider the intermediate adsorbed species that have strongest adsorption energies, since those are expected to have the dominant surface concentration (θ) and, thus, contribute more to the reaction rate. Thus, in the present case one would attempt to design a WGS reaction path using b-CO, b-H, bi-COOH and l-OH adsorbed intermediate species. However, since it is possible that some of these intermediates are in fact spectator species, spectroscopically observable intermediates that do not contribute to the catalytic activity, we consider all possible reaction intermediates found in section 3.1 to model the WGS mechanistic path. Spectator species may be intermediates with strong binding energies to the surface, and may inhibit subsequent reaction steps and in some cases even cause catalysts surface poisoning and deactivation. Considering the existence of spectator species in heterogeneous catalytic reactions, one can define a *kinetic* and a *thermodynamic* path for a particular reaction mechanism.[58] Since the catalytic activity is represented by the

kinetic path we first screen the various mechanistic pathways to locate the intermediates of the kinetic path and then subsequently explicitly compute the activation barrier for each mechanistic step. It is noted that our computational treatment here explicitly takes into account possible intermolecular interactions between co-adsorbed intermediate species.

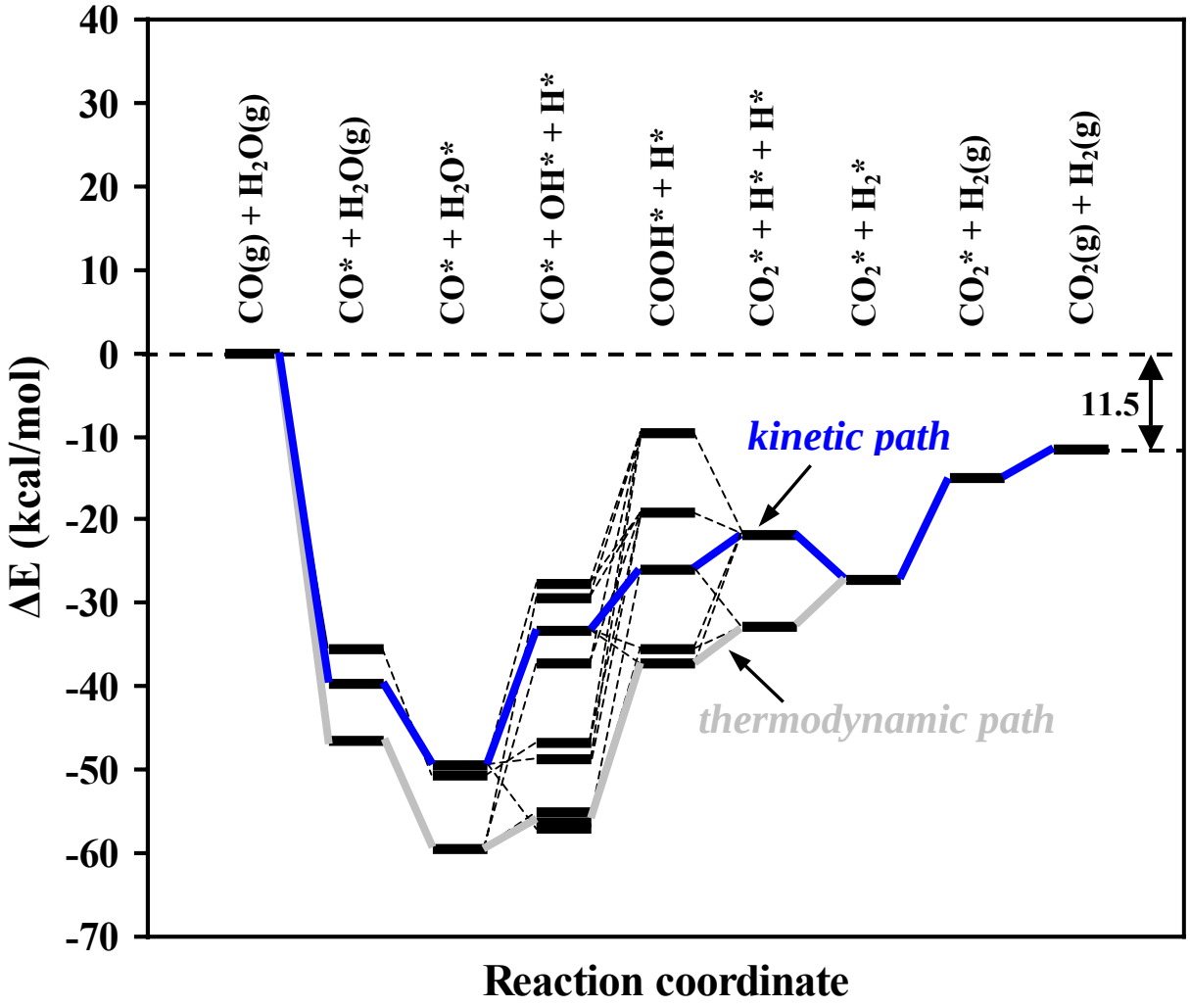

Figure 5: Potential energy diagram of the various reaction paths the WGS reaction can follow on the $Rh_4(3,1)$ cluster. The *kinetically* and the *thermodynamically* favored paths are shown in red and green, respectively. Energies of the WGS reaction reactant and products were computed by restricting the relative intermolecular and adsorbate-to-cluster separation to 10 Å. Energies of the various intermediates and the possible reaction paths can be found in the supporting information section S-Table 3 and S-Table 4, respectively.

Initially, optimized geometries and energies of all co-adsorbed intermediates (S-Table 3) using the postulated WGS reaction mechanism and the various possible intermediate configurations (Fig. 2) were located. To our advantage, certain combinations of co-adsorbed intermediates in their initial state were not stable, and thus transformed to existing more stable configurations. This resulted in a decrease of the various combinations of co-adsorbed intermediate species from 42 to 25. For example, co-adsorbed **h-H** and **l-H** spontaneously transformed to **b-H,** whereas **h-CO** was usually not stable and transformed into **b-CO**. The 25 co-adsorbed intermediates were then used to study the energetics of the various mechanistic paths (S-Table 4) of the WGS reaction. These resulted in 34 possible mechanistic paths on the $Rh_4(3,1)$ cluster which are presented in Fig. 5. It is evident that explicit computation of all activation energy barriers was computationally prohibitive, thus the various pathways were screened for the one relevant to the catalytic activity, named the *kinetically favored path* or *kinetic path*, with the use of two selection criteria: (i) the reaction paths that have the lowest E_a for their RDS, given from Brønsted–Evans–Polanyi (BEP) relationships[59, 60] were first located, (ii) a form of the Sabatier principle[61] was then used for the mechanistic paths that have the same E_a for their RDS. It is noted that BEP relationships are empirical equations that correlate the activation energy (E_a) to ΔG for an elementary reaction step. Recently, it has been demonstrated through first principle computations that analogous equations exist between E_a and the enthalpy and energy change (ΔH, ΔE) in dissociation and association reactions occurring on heterogeneous catalysts. [62-64] These equations are particularly useful when estimation of activation energy barriers[65] is desirable or when catalytic activity variations[64] are to be rationalized. Equations appear to be universally applicable

to a broad range of reactions (e.g. oxidation, hydrogenation, dissociation, association) of various adsorbates (e.g. CO, CO_2, NO, N_2O, H_2O) undergoing chemical reactions on various transition metals. Estimates of the activation energy barriers were obtained from the following expression (derived in appendix),

$$E_a = \alpha \cdot E_2 + c - E_1 \tag{3}$$

where E_1 and E_2 are the intermediate energies of a reaction step with respect to the reactants in their standard states (CO_{gas}, H_2O_{gas}), and α = 0.92 and c = 0.87eV determined by Michaelides *et al.*[63] It is noted that the screening for the kinetic path is not very sensitive to the absolute values of the BEP constants (α and c). For the barrier-less reaction steps, such as the adsorption/desorption of reactants/products, α and c were set to zero.

The Sabatier principle[61] states that an efficient catalyst is one where the adsorbate-surface interactions are of intermediate strength. Interactions of intermediate strength indicate that the gas phase molecules interact with the catalyst surface weakly to avoid poisoning (permanent binding) of active catalytic sites. In other words, the binding energy (ΔE_i) for each intermediate should be close to the total energy change for the reaction (ΔE_{WGS}) so that the intermediates of each catalytic step can undergo subsequent reactions to finally form the products without increased energy requirements. Here, the selection criterion we employ locates the reaction pathway in which the intermediates have a minimum sum (S) for their absolute adsorption energies($|\Delta E_i|$) with respect to the reactant energies to the metal cluster, given by:

$$S = \sum_{i=1}^{n} |\Delta E_i| \tag{4}$$

The screening results for the 34 pathways of the WGS reaction are given in the supporting information (S-Table 4) and show that the *kinetic path* connecting the reactants and products includes the following reaction steps:

$CO_{(g)} + H_2O_{(g)} + * \rightarrow$ l-CO* + $H_2O_{(g)}$

l-CO* + $H_2O_{(g)}$ + *$\rightarrow$ l-CO* + H_2O*

l-CO* + H_2O* + * $\rightarrow$ l-CO* + b-H* + b-OH*

l-CO* + b-H* + b-OH* $\rightarrow$ carb-COOH* + b-H* + *

carb-COOH* + b-H* + * $\rightarrow$ CO_2* + l-H*+ b-H*

CO_2* + l-H* + b-H* $\rightarrow$ CO_2* + H_2*+ *

CO_2* + H_2* $\rightarrow$ CO_2* + $H_{2(g)}$ + *

CO_2* + $H_{2(g)}\rightarrow$ $CO_{2(g)}$ + $H_{2(g)}$ + *

This reaction mechanism is in close agreement with the mechanism Mavrikakis and co-workers recently presented for Cu(111)[14] and Pt(111)[13], although more detailed in the sense that it includes information about the relative adsorption configuration of co-adsorbed intermediates. In principle, the kinetic path of the WGS reaction on a small dimensional cluster is not necessarily the same to that on an extended surface. The highly unsaturated nature of the transition metal nanocluster may manifest lower energy pathways that may not be possible on an extended surface. For the vast majority of mechanistic paths that were found based on pure energy considerations using the two selection criteria, the dissociation of water and formate association reaction steps had the highest activation energy barriers. However, explicit computation of the free energy barriers for the *kinetic path* in the following section shows that the formate dissociation step is also important in controlling the reaction rate. On the other hand, the *thermodynamic path*, the path that interconnects all the lowest energy intermediates was found to be:

$CO_{(g)} + H_2O_{(g)} + * \rightarrow$ b-CO* + $H_2O_{(g)}$

b-CO* + $H_2O_{(g)}$ + *$\rightarrow$ b-CO* + H_2O*

b-CO* + H_2O* + *$\rightarrow$ l-CO* + b-H* + l-OH*

l-CO* + b-H* + l-OH* $\rightarrow$ bi-COOH* + b-H*+ *

bi-COOH* + b-H* + *$\rightarrow$ CO_2* + b-H* + b-H*

CO_2* + b-H*+ b-H* $\rightarrow$ CO_2* + H_2*+ *

CO_2* + H_2* $\rightarrow$ CO_2* + $H_{2(g)}$ + *

CO_2* + $H_{2(g)}\rightarrow$ $CO_{2(g)}$ + $H_{2(g)}$ + *

The drastic difference between *kinetic* and *thermodynamic* path is that in the first the reaction proceeds through a carboxylate-formate (**carb-COOH**) intermediate, whereas in the latter proceeds through a bidentate-formate (**bi-COOH**) intermediate species. Thus, it is noted that **bi-COOH** that has been previously observed by steady-state isotopic-exchange experiments may in fact be a spectator species[66] that occupies active sites on the catalyst surface without contributing to the catalytic activity. For the reaction path more relevant to the catalytic activity, the kinetic path, explicit computations of the activation energy barriers were performed which confirmed that the RDS for the WGS reaction on the Rh_4(3,1) cluster is the dissociation of water with a free energy barrier of 53.8 kcal/mol for the CO-preadsorbed mechanistic path. The energies and E_a for the complete mechanism are presented in the potential energy diagram of Fig. 6 along with the mechanism of the homogeneous WGS reaction[67, 68], which occurs in the absence of a catalyst, and it is presented in order to emphasize the catalytic effect of the transition metal cluster.

For the heterogeneous WGS reaction, the adsorption of CO occurs first due to the higher sticking coefficient of CO on rhodium compared to water. Both adsorptions are barrier-less processes although there is small free energy barrier (6.7 kcal/mol) for the

adsorption of CO due to great decrease of the entropy in the transition and adsorbed states. Based on the adsorption energies of these intermediate species, -39.7 kcal/mol and -9.8 kcal/mol, respectively, the surface concentration of CO is expected to be dominant on the cluster surface. It is noted that in the simulation, even at cluster adsorbate separations of 10Å, the molecules would move towards the cluster and adsorb. Subsequently, water dissociates to form **b-H** and **b-OH** species through a relatively high free energy barrier (24.2 kcal/mol). The latter being at an advantageous stereochemical position attacks **l-CO** to form **carb-COOH** which then dissociates to form **l-H** and adsorbed $\mathbf{CO_2}$ with a free energy expense of 25.9 and 26.9 kcal/mol, respectively. Finally, the two atomic hydrogen species located on adjacent positions have to overcome a free energy barrier of 1.7 kcal/mol in order to form molecularly adsorbed $\mathbf{H_2}$ which along with $\mathbf{CO_2}$ desorb through a barrier-less step to form the gas-phase $CO_{2(g)}$ and $H_{2(g)}$ products. It is evident that the 4-fold stronger adsorption energy of CO compared to H_2O on the present rhodium nanocluster will cause most of the metal particle sites to be occupied by CO. Thus, CO may actually act as a poison for the particular reaction since it prohibits water from adsorbing and dissociating. This observation is in agreement with the relative activity of transition metals towards the low-T WGS reaction, in which metals such as Cu (21.3 kcal/mol) and Au(27.0 kcal/mol) which are known to be the most active catalysts have low adsorption energies for CO, whereas metals such as Ir (56.9 kcal/mol) and Rh (36.1 kcal/mol) exhibit only weak activity.[40] This explanation is also in agreement with various kinetic studies of the WGS reaction that exhibit a rate expression that is zeroth-order with respect to the partial pressure of CO.[69-71] It is evident that higher water vapor pressures compared to the partial pressure of CO are beneficial for increasing

the WGS reaction rate since this would increase the relative surface concentration of water (θ_{H2O}) with respect to CO (θ_{CO}) on rhodium. Furthermore, the adverse effect that adsorbed CO has onto the free energy barrier for the dissociation of water is further emphasized in Section 3.3, where we observe a dramatic decrease of the barrier in the absence of co-adsorbed CO due to a presumable electronic effect.

For the homogeneous WGS reaction the mechanism proceeds through a formic acid (HCOOH) intermediate as initially suggested from first principles computations[68] and recently confirmed by Nuclear Magnetic Resonance (NMR) experiments[72] with isotopically labeled ^{13}CO. In particular, the mechanism proceeds through a high free energy TS (64.3 kcal/mol) which results in the formation of cis-HCOOH after dissociation of an O-H bond (RDS). Then cis-HCOOH undergoes an internal rotation by 180° of the C-OH bond, to form trans-HCOOH with relatively low energy requirements (12.2 kcal/mol). Finally, trans-HCOOH dissociates into molecular hydrogen and carbon dioxide through a high-energy TS with an activation energy barrier of 63.1 kcal/mol.

On one hand the homogeneous WGS reaction has a higher E_a for the RDS (64.3 kcal/mol) and also follows a high-energy path compared to the heterogeneous WGS reaction. Thus, elevated temperatures and pressures are necessary in order to achieve considerably high reaction rates. On the other hand, the heterogeneous WGS reaction follows a lower energy reaction pathway, one that consists of many more reaction steps with lower activation energy barriers. The transition metal particle offers stabilization to two new intermediate and transition state structures due to its highly uncoordinated electronic structure. This picture is in agreement with the Taylorian[73] specific reactive site view rather than the Langmuirian[74] uniform surface view in which reaction rates are

controlled by defects and highly uncoordinated sites that are sometimes present only in small numbers, rather than extended defect-free surfaces.[58]

We suggest that lowering of the energetic barrier for dissociation of water will significantly affect the reaction rate and consequently the turn-over-frequency (TOF) of the catalyst for the low-T WGS reaction.

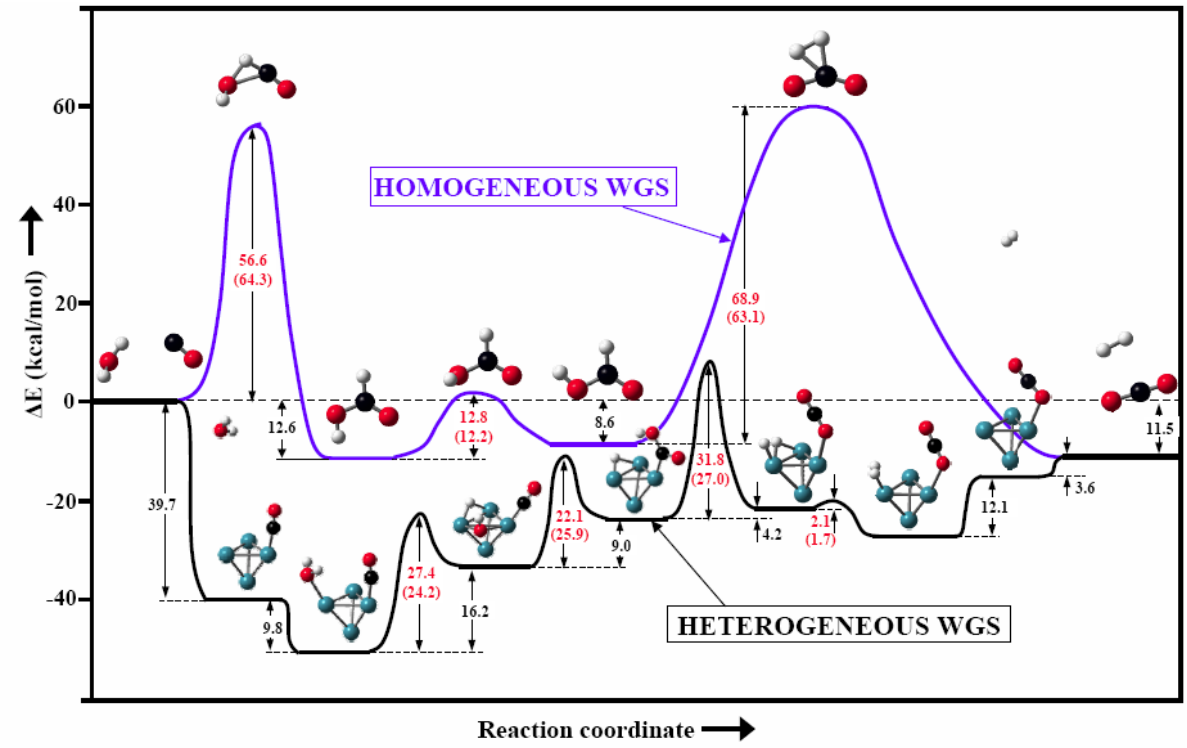

Figure 6: Potential energy diagram of the kinetic path of the WGS reaction on the $Rh_4(3,1)$ cluster (black) and in gas phase (blue) through an associative formate mechanism at standard temperature and pressure. Values in parenthesis are the corresponding free energy barriers ($\Delta G^{\ddagger}$) at STP. The energy values for the heterogeneous and homogeneous WGS reactions are given in the supporting information S-Table 5a and S-Table 5b, respectively. Details of the formate association have been omitted for better clarity.

3.3 Water-promoted mechanism of the low-T WGS reaction

Co-adsorbed water has been previously shown to have a promoting effect in CO oxidation[75] and the dissociation of water on metal surfaces.[76, 77] Furthermore, Raman

spectroscopy experiments revealed water density effects which enhance the kinetics of the homogenous WGS reaction.[78] Mechanistically, this has been explained through the stabilizing effect water can have onto the formic acid transition state through H-bonding.[79]

Here we explore the effect of co-adsorbed water on the water dissociation elementary reaction of the heterogeneous low-T WGS reaction presented in section 3.2. In general, water is known to wet metal surfaces by forming hexagonal adlayers, either from experimental[43, 46, 48, 80] or computational[44] studies. Thus, we explore if an H-bonded network could cause lowering of the activation energy barrier for water dissociation. We test this hypothesis on four water cluster model systems (Fig. 7) to assess the effect of linear and cyclic H-bonded water networks on the barrier (E_a) for water dissociation. The water networks studied were of dimeric, trimeric or hexameric form, although other stable clusters might be envisioned. In particular, we find that the $\Delta G^{\ddagger}$ ($\Delta E^{\ddagger}$) values for the monomeric, dimeric and trimeric water/cluster systems are: 20.0 (23.1), 16.9 (20.7) and 17.3 (20.6) kcal/mol, respectively. A stable hexameric water cluster was also located (Fig. 7d) similar to the hexagonal adlayers observed on extended surfaces. However, computation of the TS structure was prohibitive to us.

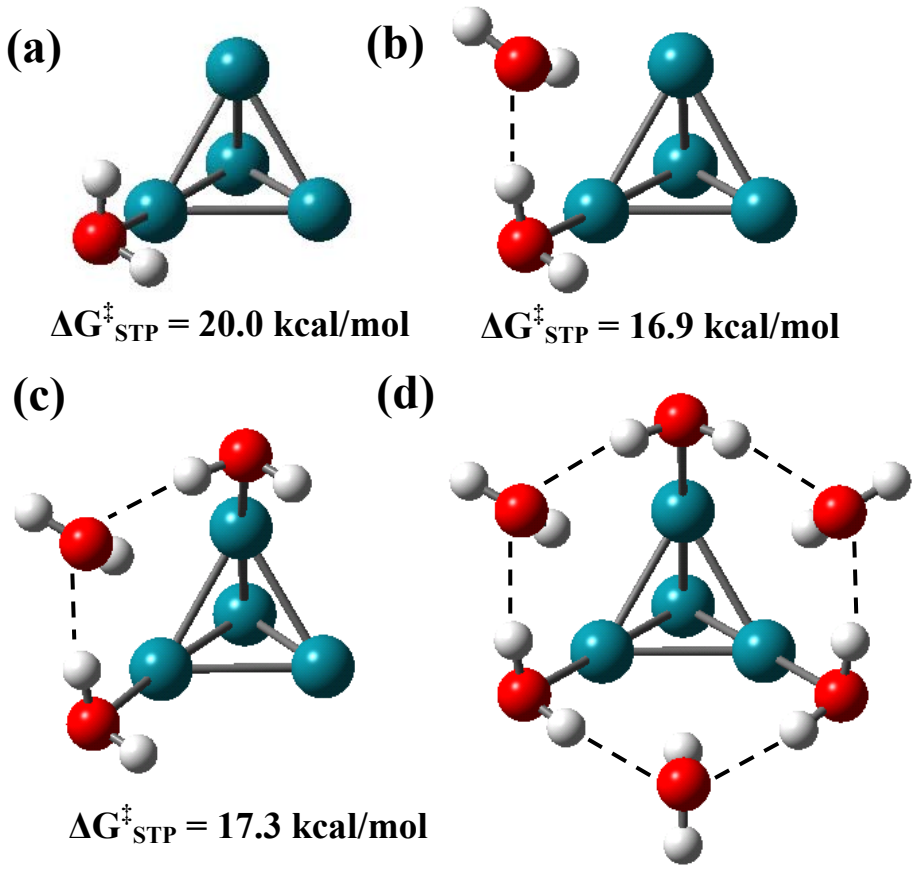

Figure 7: Various stable water clusters of (a) monomeric, (b) dimeric, (c) trimeric and (d) hexameric form, wetting $Rh_4(3,1)$ metal cluster. Grey, light grey and white correspond to oxygen, rhodium and hydrogen, respectively. The Rh cluster coordinates before and after water dissociation and the transition states can be found in the supporting information (S-Table 5).

Comparison of the free energy of the barrier for water dissociation (20.0 kcal/mol) and water-mediated water dissociation (~16.9 kcal/mol) shows a lowering of the activation energy barrier by 3.1 kcal/mol (~16%). A similar effect has been observed on water dissociation on Ru{0001}, where water incorporated in a water bilayer has a 8.2 kcal/mol lower energetic barrier for water dissociation.[81] The decrease of the free energy barrier is about the same as the interaction energy (H-bond) between the water dimer in gas phase (3.4 kcal/mol). Additional decrease of the free energy barrier for water

dissociation was not observed for the trimeric water clusters due to a presumable multiple H-bond effect on the water dissociation transition state. This clearly suggests that the H-bond interaction weakens the O-H bond of the dissociating water molecule causing, therefore, a promoting effect. Such a promoting effect for the WGS reaction is pointed out *for the first time*, although there is experimental evidence that water can have a promoting effect onto the WGS reaction rate.[52] In the particular study, the authors attributed the promoting effect of water to be the result of a stabilizing effect of water on a formate transition state located at the substrate without providing further evidence. Here, on the other hand we show that water can have this promoting effect through a reaction mechanism that explicitly occurs on the transition metal cluster and likely on an extended surface. The basic mechanism for the water dissociation is demonstrated in Scheme 2, where hydrogen in an attempt to detach from oxygen initially forms a temporary Zundel-cation[82] ($H_5O_2^+$) which consists of a hydronium ion (H_3O^+) hydrogen-bonded to the donor water, which then decomposes to form a **b-H** intermediate on the metal cluster.

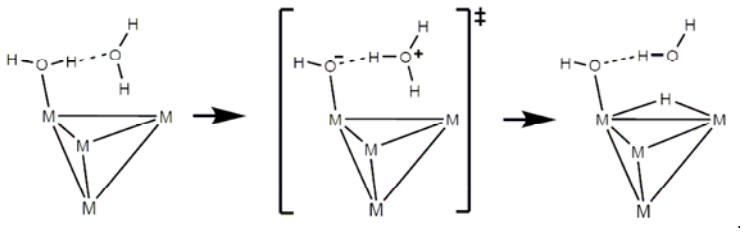

Scheme 2: Simplified schematic of water-promoted dissociation of water on transition metal clusters.

Apart from the energetic advantage (lower $\Delta G^{\ddagger}$) of this mechanism, the hydrogen cation is brought in close proximity to its final stereochemical position. Furthermore,

efficient H-tunneling between water molecules is evident due to the narrow FWHM of the water-promoted barrier for dissociation compared to plain water dissociation. The water-promoted mechanism that we suggest here for the WGS reaction is also in agreement with kinetic studies[69, 70] that exhibit kinetic reaction rates of the form, $R = k \cdot P^{0}_{CO} \cdot P^{1/2}_{H2O}$ where the partial pressure of water has an order of ½ , which may be suggestive that two water molecules are necessary for every water dissociation as shown in Scheme 2. Using the rate constant expression obtained from transition-state theory[83], $k = (k_B T/h)\exp(-\Delta G^{\ddagger}/RT)$, where k_B and h are Boltzmann and Planck constants, respectively, we calculate the rate constant for the water dissociation elementary reaction (Fig. 8). The turnover frequencies for the regular ($l\text{-}CO^* + H_2O^* + * \rightarrow l\text{-}CO^* + b\text{-}H^* + b\text{-}OH^*$), the water-promoted ($l\text{-}CO^* + 2H_2O^* + * \rightarrow l\text{-}CO^* + b\text{-}H^* + b\text{-}OH^* + H_2O^*$) and the preadsorbed water-promoted ($2H_2O^* + * \rightarrow b\text{-}H^* + b\text{-}OH^* + H_2O^*$) mechanisms were found to be 50, 500 and 100000 1/s, respectively. Comparison of the kinetic rates for the first two mechanisms show that there is a ten-fold increase of the turnover frequency due to the promoting effect of co-adsorbed water. This explains the positive kinetic order for water observed experimentally for the low-T WGS reaction and suggests that the higher turnover frequencies are attained when $P_{H2O} >> P_{CO}$, since the later inherently will have higher surface coverages. Comparison of the kinetic rates for second and third mechanisms clearly suggest that the catalytic turnover frequency can be greatly enhanced by a presumable preadsorbed water-promoted mechanism which enhances the rate constant for water dissociation by a factor of 2000. Such a mechanism is conceivable if the reactants feeds are introduced in a cyclic fashion in which water is initially preadsorbed and then exposed to a CO rich feed.

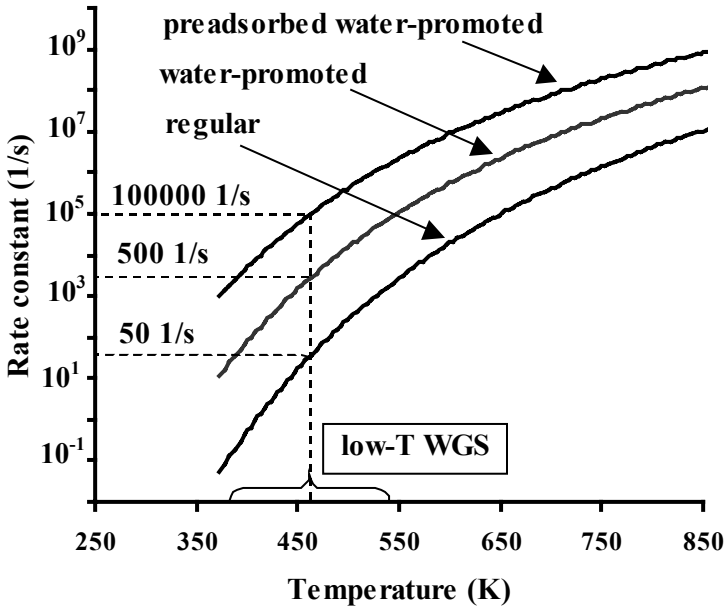

Figure 8: Transient rate constants (k) as a function of temperature for the WGS reaction under various conditions on a $Rh_4(3,1)$ cluster. The preadsorbed water-promoted, water-promoted and regular low-T WGS mechanisms represent the various conditions before and during the catalytic cycle and where found to have TOFs of 10000, 500 and 50, respectively. In the first the catalytic system is first saturated with water and then exposed to CO, in the second water and CO ae co-adsorbed but $P_{H2O} >> P_{CO}$ and in the third water and CO are co-adsorbed but $P_{H2O} \approx P_{CO}$.

Furthermore, it is suggested that future efforts in finding more efficient catalysts for a low-T WGS reaction should optimize the catalytic systems in order *to lower the* $\Delta G^{\ddagger}$ *for the dissociation of water* and at the same time keep the *adsorption energy of CO low enough* so that poisoning of active metal particle sites will not prohibit chemisorption of water and additionally affect its dissociation kinetics due to electronic reasons. Preliminary results under current investigation show that bimetallic nanoclusters in which water and CO are adsorbed on different transition metals, might be a plausible route towards this direction.

Conclusions

In the present work a detailed study of the low-T Water-Gas Shift reaction ($CO + H_2O \leftrightarrow CO_2 + H_2$) mechanism is presented on a rhodium nanocluster and the promoting effect of co-adsorbed water is explained though first principle computations. The small unsaturated nature of the small dimensional cluster offers a possibility to explore a wide variety of adsorption configurations and relevant reaction pathways for this particular chemical reaction based on the use of Bronsted-Evans-Polanyi relationships and the Sabatier principle.

The kinetically favored mechanistic path is found to proceed through a carboxylate formate intermediate and the mechanistic path located is in excellent agreement with recent findings on other transition metal surfaces (Cu, Pt). The RDS of the mechanism is the water dissociation, formate association and formate dissociation steps that have free energy barriers ($\Delta G^{\ddagger}$) of 24.2, 25.9 and 27.0 kcal/mol, respectively. We show the possibility of a preadsorbed water-mediated mechanism of the WGS reaction that causes lowering of the free energy barrier by 4.0 kcal/mol a fact that explains the positive kinetic order for water observed experimentally. Lowering the activation energy barrier for the dissociation of water and simultaneously maintaining low adsorption energies of carbon monoxide should be considered key factors in future catalyst developments for the low-temperature WGS reaction on supported-metal catalysts. Furthermore, we suggest that CO conversion turnover frequencies could be enhanced through the operation of heterogeneous low-T WGS catalysts in a cyclic fashion where water is first preadsorbed and then exposed to CO.

Acknowledgments

The Cyprus Research Promotion Foundation (CRPF) is acknowledged for financially supporting C.D.Z under the grant ΠΕΝΕΚ ΕΝΙΣΧ/0506/62. The authors thank Professor Andrew L. Cooksy and Professor Rutger A. van Santen for useful discussions and comments on the manuscript.

Supporting Information

Energies and cartesian coordinates of the various WGS intermediates and model metal water clusters and the various possible mechanistic pathways are given as supporting information (S-Table 1-6). This information is available free of charge via the Internet at http://pubs.acs.org.

Appendix

Suppose one considers a catalytic reaction that is described by an arbitrary potential energy diagram similar to that shown in Fig. 9. Travelling from the gas phase reactants to the products the adsorbed chemical species encounter initially two non-activated processes (physisorption), three activated processes, and finally another non-activated process. In other words initially the gas phase species are adsorbed to the catalyst, then they are activated by the catalyst through the lowering of activation barriers for bond breaking and bond formation reactions, and finally the products desorb again to the gas phase.

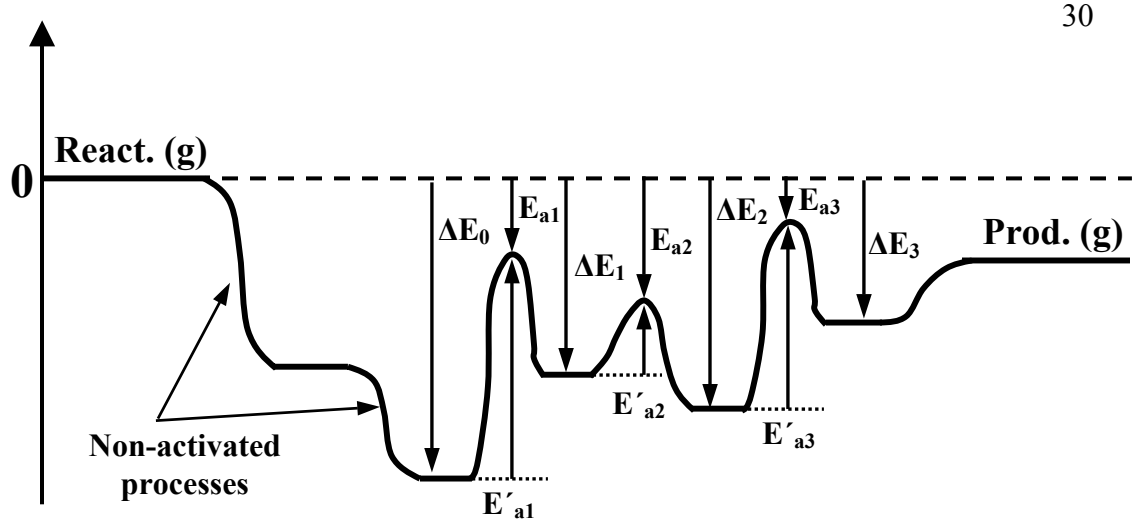

Figure 9: Arbitrary potential energy diagram for a catalytic reaction.

Assuming the existence of BEP relationships for the activated steps that involve the same intermediates (but different binding configurations), one can state that the activation energy barrier for mechanistic step 2 is given by:

$$E_{a2} = \boldsymbol{\alpha} \cdot \Delta E_2 + c \tag{5}$$

, where α and c are constants given by BEP relationships and the energy changes are given with respect to the reactants standard state:

$$\Delta E_i = E_i - E_{react.(g)} \tag{6}$$

, where E_i and $E_{react.(g)}$ are the energies of the co-adsorbed intermediates and the gas phase reactants, respectively. Since the gas phase reactants are in their standard states, $E_{react.(g)} = 0$. Therefore,

$$\Delta E_i = E_i \tag{7}$$

For the sake of simplicity, since most of the reaction steps for the WGS reaction involve X-H (where X = Oxygen or Carbon) bond breaking reactions, one can assume that α and c are the same for all activated mechanistic steps, whereas for all non-activated

processes they are just zero. This assumption is not rigorously true and has to be checked for the particular catalytic reaction at hand. However, in the case that this assumption is not valid, one can still employ a treatment where different BEP constants (α_1, c_1, α_2, c_2, α_3, c_3) for each particular step are assumed and still find a solution. The activation energy barrier for step 2 is given by the expression,

$$E'_{a2} = E_{a2} - \Delta E_1 \quad (8).$$

Combinations of Eqns. 3, 5 and 6 yields,

$$E'_{a2} = \boldsymbol{\alpha} \cdot E_2 + c - E_1 \quad (9)$$

,which correlates the activation energy barrier for a particular activated mechanistic step to the energies of the co-adsorbed intermediates of that step.

References

(1) Choudhary, T. V.; Goodman, D. W., *Catal. Today* **2002**, *77*, 65.
(2) Basagiannis, A. C.; Verykios, X. E., *Appl. Catal. A: Gen.* **2006**, *308*, 182.
(3) Chernik, S.; French, R.; Feik, C.; Chornet, E., *Ind. Eng. Chem. Res.* **2002**, *41*, 4209.
(4) Cortright, R. D.; Davda, R. R.; Dumesic, J. A., *Nature* **2002**, *418*, 964.
(5) Fu, Q.; Saltsburg, H.; Flytzani-Stephanopoulos, M., *Science* **2003**, *301*, 935.
(6) Farrauto, R.; Hwang, S.; Shore, L.; Ruettinger, W.; Lampert, J.; Giroux, T.; Liu, Y.; Ilinich, O., *Annu. Rev. Mater. Res.* **2003**, *33*, 1.
(7) Mhadeshwar, A. B.; Vlachos, D. G., *Catal. Today* **2005**, *105*, 162.
(8) Rhodes, C.; Williams, B. P.; King, F.; Hutchings, G. J., *Catal. Commun.* **2002**, *3*, 381.
(9) Greeley, J.; Jaramillo, T. F.; Bonde, J.; Chorkendorff, I.; Nørskov, J. K., *Nature Mater.* **2006**, *5*, 909.
(10) Mavrikakis, M., *Nature Mater. 5*, 847.
(11) Nørskov, J. K.; Christensen, C. H., *Science* **2006**, *312*, 1322.
(12) Gokhale, A. A.; Dumesic, J. A.; Mavrikakis, M., *J. Am. Chem. Soc.* **2008**, *130*, 1402.
(13) Grabow, L. C.; Gokhale, A. A.; Evans, S. T.; Dumesic, J. A.; Mavrikakis, M., *J. Phys Chem. C* **2008**, *112*, 4608.
(14) Gokhale, A. A.; Dumesic, J. A.; Mavrikakis, M., *J. Am. Chem. Soc.* **2008**, *130*, 1402.
(15) Kua, J.; Goddard, W. A., *J. Am. Chem. Soc.* **1999**, *121*, 10928.
(16) Liu, Z. P.; Jenkins, S. J.; King, D. A., *Phys. Rev. Let.* **2005**, *94*, 196102.
(17) Tominaga, H.; Nagai, M., *J. Phys. Chem. B* **2005**, *109*, 20415.

(18) Liu, P.; Rodriguez, J. A., *J. Phys. Chem. B* **2006**, *110*, 19418.
(19) Liu, P.; Rodriguez, J. A., *J. Chem. Phys.* **2007**, *126*, 164705.
(20) Frisch *et al.,* M. J. *GAUSSIAN03*, C.02; Gaussian Inc: Wallingford CT, 2004.
(21) Becke, A. D., *J. Chem. Phys.* **1993**, *98*, 5648.
(22) Lee, C.; Yang, W.; Parr, R. G., *Phys. Rev. B* **1988**, *37*, 785.
(23) Hu, Q.-M.; Reuter, K.; Scheffler, M., *Phys. Rev. Lett.* **2007**, *98*, 176103.
(24) Gajdoš, M.; Eichler, A.; Hafner, J., *J. Phys.: Condens. Matter* **2004**, *16*, 1141.
(25) Woon, D. E.; Dunning Jr., T. H., *J. Chem. Phys.* **1993**, *98*, 1358.
(26) Wilson, A.; van Mourik, T.; Dunning Jr., T. H., *J. Mol. Struct.* **1997**, *388*, 339.
(27) Peterson, K. A.; Woon, D. E.; Dunning Jr., T. H., *J. Chem. Phys.* **1994**, *100*, 7410.
(28) Kendall, R. A.; Jr., T. H. D.; Harrison, R. J., *J. Chem. Phys.* **1992**, *96*, 6796.
(29) Dunning Jr., T. H., *J. Chem. Phys.* **1989**, *90*, 1007.
(30) Boys, S. F.; Bernardi, F., *Mol. Phys.* **1970**, *19*, 553.
(31) Cundari, T. R.; Stevens, W. J., *J. Chem. Phys.* **1993**, *98*, 5555.
(32) Stevens, W.; Basch, H.; Krauss, J., *J. Chem. Phys.* **1984**, *81*, 6026.
(33) Stevens, W. J.; Krauss, M.; Basch, H.; Jasien, P. G., *Can. J. Chem.* **1992**, *70*, 612.
(34) Smedh, H. A. B.; Borg, M.; Nyholm, R.; Andersen, J. N., *Surf. Sci.* **2001**, *115*, 491.
(35) Peng, C.; Schlegel, H. B., *Isr. J. Chem.* **1993**, *33*, 449.
(36) Peng, C.; Ayala, P. Y.; Schlegel, H. B.; Frisch, M. J., *J. Comput. Chem.* **1996**, *17*, 49.
(37) Portmann, S.; Lüthi, H. P., *CHIMIA* **2000**, *54*, 766.
(38) McHale, J. L., *Molecular Spectroscopy*. Prentice Hall: Upper Saddle River NJ, 1999.
(39) Zeinalipour-Yazdi, C. D.; Cooksy, A. L.; Efstathiou, A. M., *J. Phys. Chem. C* **2007**, *11*, 13872.
(40) Zeinalipour-Yazdi, C. D.; Cooksy, A. L.; Efstathiou, A. M., *Surf. Sci.* **2008**, *602*, 1858.
(41) Bruce, A.; Ho, W., *J. Vac. Sci. Technol. A* **1987**, *5*, 632.
(42) Michaelides, A., *Appl. Phys. A* **2006**, *85*, 415.
(43) Michaelides, A.; Ranea, V. A.; de Andres, P. L.; King, D. A., *Phys. Rev. Lett.* **2003**, *90*, 216102.
(44) Michaelides, A.; Alavi, A.; King, D. A., *Phys. Rev. B* **2004**, *69*, 113404.
(45) Rar, A. A.; Ivanov, V. P., *React. Kinet. Catal. Lett.* **1987**, *34*, 445.
(46) Hegde, R. I.; White, J. M., *Surf. Sci.* **1985**, *157*, 17.
(47) Hedge, R. I.; White, J. M., *Surf. Sci.* **1985**, *157*, 17.
(48) Doering, D.; T.E.Madey, *Surf. Sci.* **1982**, *123*, 305.
(49) Shido, T.; Asakura, K.; Iwasawa, Y., *J. Catal.* **1990**, *122*, 55.
(50) Shido, T.; Iwasawa, Y., *J. Catal.* **1991**, *129*, 343.
(51) Shido, T.; Iwasawa, Y., *J. Catal.* **1992**, *136*, 493.
(52) Shido, T.; Iwasawa, Y., *J. Catal.* **1993**, *141*, 71.
(53) Chenu, E.; Jacobs, G.; Crawford, A. C.; Keogh, R. A.; Patterson, P. M.; Sparks, D. E.; Davis, B. H., *Appl. Catal. B* **2005**, *59*, 45.
(54) Jacobs, G.; Williams, L.; Graham, U.; Thomas, G. A.; Sparks, D. E.; Davis, B. H., *Appl. Catal. A* **2003**, *252*, 107.
(55) Chen, Y. X.; Heinen, M.; Jusys, Z.; Behm, R. J., *Langmuir* **2006**, *22*, 10399.

(56) Castner, D. G.; Sexton, B. A.; Somorjai, G. A., *Surf. Sci.* **1978**, *71*, 519.
(57) At higher temepratures one would also have to consider the a presumable redox mechanism due to the possibility of the following two elementary reaction steps: OH* $\rightarrow$ O* + H* and CO* + O* CO_2*.
(58) van Santen, R. A.; Neurock, M., *Molecular Heterogeneous Catalysis: A conceptual and computational approach*. Wiley-VCH: 2006; p 1.
(59) Brønsted, N., *Chem. Rev.* **1928**, *5*, 231.
(60) Evans, M. G.; Polanyi., N. P., *Trans. Faraday Soc.* **1938**, *34*, 11.
(61) Sabatier, P., *La catalyse en chimie organique, Bérange, Paris* **1920**.
(62) Nørskov, J. K.; Bligaard, T.; Logadottir, A.; Bahn, S.; Hansen, L. B.; Bollinger, M.; Bengaard, H.; Hammer, B.; Sljivancanin, Z.; Mavrikakis, M.; Xu, Y.; Dahl, S.; Jacobsen, C. J. H., *J. Catal.* **2002**, *209*, 275.
(63) Michaelides, A.; Liu, Z.-P.; Alavi, A.; King, D. A.; Hu, P., *J. Am. Chem. Soc.* **2002**, *125*, 3704.
(64) Logadottir, A.; Rod, T. H.; Nørskov, J. K.; Hammer, B.; Dahl, S.; Jacobsen, C. J. H., *J. Catal.* **2001**, *197*, 229.
(65) Schumacher, N. M.; Boisen, A.; Dahl, S.; Gokhale, A. A.; Kandoi, S.; Grabow, L. C.; Dumesic, J. A.; Mavrikakis, M.; Chorkendorff, I., *J. Catal.* **2005**, *229*, 265.
(66) Tibiletti, D.; Goguet, A.; Meunier, F. C.; Breen, J. P.; Burch, R., *Chem. Commun.* **2004**, *14*, 1636.
(67) Akiya, N.; Savage, P. E., *AIChE Journal* **1998**, *44*, 405.
(68) Melius, C. F.; Bergan, N. E.; Shepherd, J. E. In Proceedings of the 23rd International Symposium on Combustion, Pittsburgh, 1990; The Combustion Institute: Pittsburgh, 1990; pp 217.
(69) Hilaire, S.; Wang, X.; Luo, T.; Gorte, R. J.; Wagner, J., *Appl. Catal. A General* **2001**, *215*, 271.
(70) Grenoble, D. C.; Estadt, M. M.; Ollis, D. F., *J. Catal.* **1981**, *67*, 90.
(71) Campell, C. T.; Daube, K. A., *J. Catal.* **1987**, *104*, 109.
(72) Yoshida, K.; Wakai, C.; Matubayasi, N.; Nakahara, M., *J. Phys. Chem. A* **2004**, *108*, 7479.
(73) Taylor, H. S., *Proc. Roy. Soc. A* **1925**, *105*, 9.
(74) Langmuir, I., *Trans. Farad. Soc.* **1921**, *17*, 62.
(75) Xue-Qing, G.; Hu, P.; Raval, R., *J. Chem. Phys.* **2003**, *119*, 6324.
(76) Andersson, K.; Ketteler, G.; Bluhm, H.; Yamamoto, S.; Ogasawara, H.; Pettersson, L. G. M.; Salmeron, M.; Nilsson, A., *J. Phys. Chem. C* **2007**, *111*, 14493.
(77) Yamamoto, S.; Andersson, K.; Bluhm, H.; Ketteler, G.; Starr, D. E.; Schiros, T.; Ogasawara, H.; Pettersson, L. G. M.; Salmeron, M.; Nilsson, A., *J. Phys. Chem. C* **2007**, *111*, 7848.
(78) Rice, S. F.; Steeper, R. R.; Aiken, J. D., *J. Phys Chem. A* **1998**, *102*, 2673.
(79) Wang, B.; Hou, H.; Gu, Y., *Chem. Phys. Chem.* **1999**, *243*, 27.
(80) Michaelides, A.; Morgenstern, K., *Nature Mater.* **2007**, *6*, 597.
(81) Michaelides, A.; Alavi, A.; King, D. A., *J. Am. Chem. Soc.* **2003**, *125*, 2746.
(82) Zundel, G.; Metzger, H., *Z. Phys. Chem.* **1968**, *58*, 225.
(83) Kramers, H. A., *Physica* **1940**, *7*, 284.